Title

Single-cell profiling of D-2-hydroxyglutarate using surface-immobilized resazurin analogs

Authors

Cheng, Hanjun
Li, Zhonghan
Guo, Zhili
et al.

Publication Date

2021-10-01

DOI

10.1016/j.bios.2021.113368

Peer reviewed

HHS Public Access

Author manuscript

Biosens Bioelectron. Author manuscript; available in PMC 2022 October 15.

Published in final edited form as:

Biosens Bioelectron. 2021 October 15; 190: 113368. doi:10.1016/j.bios.2021.113368.

Single-cell profiling of D-2-hydroxyglutarate using surface-immobilized resazurin analogs

Hanjun Cheng[#a], **Zhonghan Li**[#b], **Zhili Guo**[b], **Shiqun Shao**[a], **Li Mo**[c], **Wei Wei**[a,c,*], **Min Xue**[b,*]

[a]Institute for Systems Biology, Seattle, Washington 98109, United States.

[b]Department of Chemistry, University of California, Riverside, Riverside, California 92521, United States.

[c]Department of Molecular and Medical Pharmacology, University of California, Los Angeles, California 90095, United States.

[#] These authors contributed equally to this work.

Abstract

D-2-hydroxyglutarate (D2HG) is over-produced as an oncometabolite due to mutations in isocitrate dehydrogenases (IDHs). Accumulation of D2HG can cause the dysfunction of many enzymes and genome-wide epigenetic alterations, which can promote oncogenesis. Quantification of D2HG at single-cell resolution can help understand the phenotypic signatures of *IDH*-mutant cancers and identify effective therapeutics. In this study, we developed an analytical method to detect D2HG levels in single cancer cells by adapting cascade enzymatic reactions on a resazurin-based fluorescence reporter. The resazurin probe was immobilized to the sensing surface via biotin-streptavidin interaction. This surface chemistry was rationally optimized to translate the D2HG levels to sensitive fluorescence readouts efficiently. This D2HG assay demonstrated good selectivity and high sensitivity toward D2HG, and it was compatible with the previously developed single-cell barcode chip (SCBC) technology. Using the SCBC platform, we performed simultaneous single-cell profiling of D2HG, glucose uptake, and critical oncogenic signaling proteins in single *IDH*-mutant glioma cells. The results unveiled the complex interplays between metabolic and oncogenic signaling and led to the identification of effective combination targeted therapy against these *IDH*-mutant glioma cells.

Keywords

D-2-hydroxyglutarate; oncometabolite; fluorescence; enzymatic assay; single-cell analysis

[*]Corresponding authors wwei@systemsbiology.org, minxue@ucr.edu.

Declaration of Competing Interest

The authors declare that they have no known competing financial interests or personal relationships that could have appeared to influence the work reported in this paper.

1. Introduction

Cancer cells are known to exhibit altered metabolic patterns. The majority of cancer metabolism research focused on the proliferative aspect, where many critical oncogenic signaling pathways converge to adapt cancer cell metabolism to incorporate nutrients into biomass for abnormal proliferation efficiently.(Cairns et al. 2011; Ward and Thompson 2012) Representative examples are hyperactive aerobic glycolysis and increased glutamine uptake,(Altman et al. 2016; Vander Heiden et al. 2009) which can generate building blocks for sustaining cell growth. Despite that the proliferative metabolism is a unifying feature of cancer cells, recent advances in high-throughput omics technologies have portrayed a more complex picture of tumor metabolism. Specifically, mutations in metabolic enzymes can lead to over accumulation of specific metabolites, which can act as signaling molecules and induce epigenetic modifications.(Schulze and Harris 2012; Thompson 2009; Ward and Thompson 2012) These abnormalities can then drive cell transformation and directly contribute to oncogenesis. Therefore, these metabolic intermediates are called oncometabolites and are essential biomarkers in cancer.(Yang et al. 2013) Analysing these oncometabolites can help reveal the cancer cells' properties and potentially lead to better therapeutic strategies.

D-2-hydroxyglutarate (D2HG) is a representative oncometabolite that arises from mutations in the isocitrate dehydrogenase (IDH) enzymes.(Dang et al. 2009; Fan et al. 2015; Mullen and DeBerardinis 2012; Xu et al. 2011; Ye et al. 2013) These mutations are prevalent in many types of cancer. For instance, more than 70% of grade II/III gliomas and around 40% of chondrosarcoma cases harbor R132 mutations on IDH1.(Mondesir et al. 2016) Similarly, more than 20% of angioimmunoblastic T-cell lymphoma cases exhibit R140/172 mutations on IDH2.(Mondesir et al. 2016) These IDH mutations cause excessive production and accumulation of D2HG from the alpha-ketoglutarate (αKG) precursor. The D2HG accumulation interferes with the function of more than 60 known dioxygenases that utilize αKG as a co-substrate, leading to genome-wide epigenetic alterations that result in cellular transformation and tumorigenisis.(Loenarz and Schofield 2008; Tahiliani et al. 2009; Tsukada et al. 2006; Xu et al. 2011)

Many studies have demonstrated the detection of D2HG in biological samples, where magnetic resonance spectroscopy, enzyme assays, and mass spectrometry are the most common tools.(Balss et al. 2012; Dang et al. 2009; Fan et al. 2015; Fu et al. 2015; Gross et al. 2010; Lin et al. 2015; Xu et al. 2011) Nevertheless, these methods are limited to bulk-level analysis. Increasing evidence has proved that tumor cells are highly heterogeneous, (Almendro et al. 2013; Nowell 1976; Polyak 2014; Quail and Joyce 2013) where considerable levels of heterogeneity manifest in the metabolic pathways and patterns, even in the isogenic tumor cell population.(DeBerardinis and Thompson 2012) Dissecting this heterogeneity is necessary for the precise identification of different phenotypes and subpopulations.(Heath et al. 2016) Therefore, the ability to analyze D2HG at single-cell resolution promises a better understanding of the *IDH*-mutant cancer cells.

Metabolic reprogramming, such as the one observed with D2HG accumulation, is critical to support malignant transformation and tumor progression, but at the same time, renders

tumors more vulnerable to metabolic perturbations.(Schulze and Harris 2012; Thompson 2009) However, the complex interplay between oncogenic signaling and metabolic pathways contributes to the tumor metabolic flexibility that alleviates this vulnerability.(Li et al. 2018; Li et al. 2019; Pavlova and Thompson 2016) This flexibility can in part clarify why some drugs, such as antimetabolites and enzyme inhibitors, do not elicit a general therapeutic efficacy, despite the universal requirement of elevated biomass synthesis. Therefore, elucidating how metabolic patterns interact with oncogenic signaling across a statistical number of single cells can help unveil network connections underlying different subpopulations, facilitating the rational design of precision therapeutic strategies. Such a task calls for an integrated bioanalytical platform that can profile small molecule metabolites and quantify oncogenic signaling proteins in the same single cells.

To achieve the goal above, we have developed the single-cell barcode chip (SCBC) technology, which enables simultaneous analysis of small molecule metabolites and proteins through a collection of orthogonal surface chemical approaches.(Li et al. 2018; Xue et al. 2016; Xue et al. 2015) This technology has helped us unveil critical interactions between various metabolic pathways and oncogenic signaling axes to reveal novel therapeutic combinations. Herein, we demonstrate a surface-based D2HG assay that is compatible with the SCBC technology. By integrating this assay with quantification of glucose uptake and signaling phosphoproteins at the single-cell level, we further demonstrate the analysis of the relationships between cell metabolism, oncogenic signaling, and cell proliferation in an *IDH*-mutant human glioblastoma cell line.

2. Material and methods

Chemicals and reagents

(2-(1H-benzotriazol-1-yl)-1,1,3,3-tetramethyluronium hexafluorophosphate (HBTU), Fmoc-Lys(alloc)-OH and Fmoc-Gly-OH were purchased from Chem-Impex (Wood Dale, IL). Rink amide MBHA resin (0.678 mmol/g, 100–200 mesh) was ordered from Aapptec (Louisville, KY). Fmoc-PEG5-OH and Fmoc-PEG24-OH were purchased from BroadPharm (San Diego, CA). Tetrakis(triphenylphosphine)palladium(0) [$Pd(PPh_3)_4$] (Strem Chemical, Inc), Phenylsilane (PhSiH3) (TCI, AmericaTM), Diisopropylethylamine (DIEA) (ACROS), Trifluoroacetic acid (TFA) (Oakwood Chemical), Bovine serum albumin (BSA), N, N-Dimethylformamide (DMF) and Acetonitrile were purchased from Fisher Scientific. Piperidine was purchased from Alfa Aesar (Ward Hill, MA). Beta-Nicotinamide adenine dinucleotide sodium salt (NAD+, 95%), D-2-hydroxyglutarate (D2HG), and biotin were obtained from Sigma-Aldrich (Saint Louis, MO). Diaphorase was obtained from Innovative Research, Inc. (Novi, MI). Active D2HG dehydrogenase (D2HGDH) was obtained from BioVision (Milpitas, CA). ssDNA-antibody conjugates, ssDNA-streptavidin conjugate, and other SCBC experiment related reagents were prepared following established protocols. (Kwong et al. 2009; Reznik et al. 2001; Xue et al. 2015)

Synthesis of Biotin-PEG5-Resazurin (BPRz)

The BPRz sequence was synthesized on Rink amide MBHA resin (200 mg, loading capacity 0.678 mmol/g) following standard solid-phase peptide synthesis protocols.(Li et al. 2018)

The synthetic scheme is shown in the Supplementary Material (Figure S1). For Fmoc deprotection, the resin was agitated with piperidine (5 mL, 20% v/v in DMF, 3× 5 min) and washed with DMF (5× 5 mL). For amino acid coupling, a solution of Fmoc-amino acid (0.68 mmol, in 3 mL of DMF), HBTU (3.2 mL of 0.2 M in DMF) and DIEA (0.28 mL) was added to the resin and agitated at room temperature for 1 h, followed by DMF washes (5× 5 mL). For the deprotection of the alloc group, the resin was agitated with a degassed solution of $Pd(PPh_3)_4$ (31 mg, 27 μmol), $PhSiH_3$ (660 uL, 5.4 mmol) in dry DCM (3 mL) at rt for 2 hours then the resulting dark solution was drained, and the resin was washed sequentially with DMF (5× 5 mL), chelating solution (Sodium diethyldithiocarbamate (5% w/v), DIEA (5% v/v) in DMF (5× 5 mL), and DMF (5× 5 mL). To cleave the peptide from the resin, a mixture of TFA and water (95:5 v/v, 10 mL) was added to the resin and agitated for 2 hours, followed by precipitation in ether. The collected and dried precipitate was further purified by reverse-phase HPLC. ESI-TOF, $C_{44}H_{62}N_8O_{15}S$, $[M+H]^+$ calculated 975.41, found 975.41 (Figure S2, S3).

Synthesis of Biotin-PEG48-Resazurin (BP2Rz)

The synthetic scheme is shown in the Supplementary Material (Figure S4). The BP2Rz was synthesized with the same procedure as BPRz at the same scale (200 mg Rink amide MBHA resin, 0.678 mmol/g). The conjugation time for Fmoc-PEG24-OH was extended to 2 hours, and for the 2nd Fmoc-PEG24-OH, double coupling (two rounds) was taken. For the cleavage cocktail, only water was utilized as a scavenger since the resazurin is not compatible with commonly used alkyl silanes (TES or TIPS). The final product was purified by reverse-phase HPLC. ESI-TOF, $C_{133}H_{239}N_9O_{59}S$, $[M+3H]^{3+}$ calculated 980.86, found 980.86 (Figure S5, S6).

Solution-phase D2HG assay

A solution of NAD+ (1 mM in PBS, 107 μL), BPRz or BP2Rz (20 μM in PBS, 100 μL) with or without streptavidin (BPRz: streptavidin = 4:1), 1 μL of diaphorase (1 kU/mL in PBS) and 2 μL of D-2HGDH (1 U/mL in PBS) was added into a well of 96-well plate. 40 μL of D-2HG solutions (various concentrations in PBS) were then added and incubated for one hour. The fluorescence intensity was then measured by a microplate reader (excitation 540 nm, emission 590 nm). The experiment was carried out in quadruplets to determine the error range.

Surface-based D2HG assay

A 16-well PDMS slab was placed onto a microscope glass slide, on which single-strand DNA oligomers were patterned in 20 μm stripes. The volume of each well was 50 μL, and it was equipped with at least eight sets of DNA barcode strips. 50 μL of streptavidin-DNA (100 nM) in 1 % BSA/PBST was added to each well, and the device was incubated at room temperature for one hour. Afterward, the solution was removed, and each well was washed with PBST three times. 45 uL of the BP2Rz (10 μM in 1% BSA/PBST) solution was added into each well and incubated at 37°C for one hour. Subsequently, each well was washed with PBST three times. At this stage, the BP2Rz probe was immobilized onto the surface and ready to use.

To obtain the standard curve for D-2HG quantification, 20 uL of NAD+ solution (1 mM in PBST), 2 μL of D2HGDH solution (1 U/mL in PBS), 2 μL of diaphorase solution (1 kU/mL in PBS) and 20 μL of D2HG solution (various concentrations in PBST) was added to each well, and the device was incubated at room temperature for one hour. The solutions were then removed, and the device was washed with 1% BSA/PBST three times, followed by three times of PBST. The PDMS slab was then removed, and the glass slide was washed in PBS, 50% PBS/water and water and then spin-dried. The surface fluorescence intensity was then measured by a microarray scanner (Genepix). Each data point was collected in quadruplets to obtain the error bar.

Cell culture

BT142 mut/- cells were purchased from ATCC (the American Type Culture Collection) and cultured in Dulbecco's Modified Eagle Media (DMEM/F12) with an additional supplement of 0.9% glucose, 4 mM L-glutamine, 25 μg/mL insulin, 100 μg/mL transferrin, 20 nM progesterone, 15 μM putrescine, 30 nM selenite, 100 U/mL of penicillin-streptomycin, and 250 ng/mL Amphotericin B in a humidified 5% CO_2 (v/v) incubator at 37 °C.

Single-cell metabolic/proteomic measurements

The adapted single-cell barcode chips (SCBCs) were fabricated according to well-established procedures.(Li et al. 2018; Xue et al. 2016; Xue et al. 2015) In brief, the D2HG surface probe BP2Rz along with the DNA-encoded antibody library (DEAL) was grafted onto the surface through DNA hybridization to generate biosensor arrays.(Li et al. 2018)

The SCBC experiment was performed following established protocols (Supplementary Material Figure S7) with slight modifications.(Li et al. 2018) To prepare single-cell suspensions for the SCBC measurements, the collected BT142 mut/- neurospheres were triturated by pipetting up and down until a single cell suspension was obtained. Followed by the addition of Blu-bio to 10 μg/mL, the resultant single-cell suspension (1 M/mL) was cultured at 37 °C for 30 min. After washed with cold PBS for 3 times, the collected BT142 mut/- was resuspended in serum-free, biotin-free media, which contained 0.1 μg/mL D2HGDH and 25 U/mL diaphorase. The generated BT142 mut/- single-cell suspension (1 M/mL) was subsequently introduced into the SCBC platform, and the relevant multiplexed metabolic/proteomic measurements were carried out via previously established protocols. It is worth noting that after the trapped single cells were lysed, the SCBC chips must be placed in a humidified oven at 37 °C to allow for the occurrence of desired cascade enzymatic reactions due to the low activity of the adapted D2HGDH.

Statistical analysis

The single-cell data was processed using OriginPro 2019b® software. The dataset was first standardized to obtain Z scores of each analyte datapoint. For agglomerative hierarchical clustering, the Euclidean distance values between single-cell data points were calculated to generate a distance matrix. This matrix was then clustered using Ward's method. For principal component analysis, the standardized single-cell dataset was processed using the software, and the loading plots were generated for PC1&PC2 and PC3&PC4. For correlation analysis, the pairwise correlation was calculated among analytes using Spearman's rank

method. Only significant correlations (with Bonferroni correction) were kept for plotting the correlation network.(Krzywinski et al. 2009)

Drug synergy test

The drug synergy test was conducted using 96-well plates. These plates were pre-coated with laminin to ensure cell adhesion. 100 μL of 10 μg/mL laminin was first added into each well of a 96-well plate, and the plate was incubated at 37°C overnight. After the plate was washed with PBS 3 times, 100 μL of BT142 mut/- single-cell suspension at 50K/mL was added into each well, and the plate was incubated at 37 °C overnight. When the BT142 cells successfully attached to the microwells, the media were changed to fresh ones (200 μL/well) containing various concentrations of Ivosidenib and LY2584702.(Hollebecque et al. 2014; Roboz et al. 2020) The cells were cultured for another 72 hours, during which time the drugs were replenished every 48 h. Subsequently, 20 μL of 0.2 mg/mL resazurin PBS solution was added into each well, followed by incubation at 37 °C for 5 hours. The resulting fluorescent signals were quantified by a plate reader (530 nm excitation / 590 nm emission).

The synergy scores of the two drugs were calculated by using the following equation:

$$S_{A,B} = I_{A,B} - (I_A + I_B - I_A \times I_B)$$

where $S_{A,B}$ is the synergy effect between drugs A and B, $I_{A,B}$ is the cell-killing efficiency by using the combination of drug A and B, while I_A and I_B are the cell-killing efficiencies from independent doses of drug A or B, respectively.

3. Results and discussion

Detection scheme

D2HG is a redox-active metabolite that can be oxidized to generate αKG.(Xu et al. 2011; Ye et al. 2013) Therefore, we can leverage the well-established coupled enzymatic reactions to assay D2HG. As shown in Figure 1a, the enzyme D2HG dehydrogenase (D2HGDH) catalyzes the transformation from D2HG to αKG, while converting NAD^+ to NADH.(Lin et al. 2015) This generated NADH can fuel a diaphorase-catalyzed redox reaction, where a resazurin analog is reduced to a highly fluorescent resorufin analog. By grafting the resazurin analog onto the surface and performing these coupled enzymatic reactions in the microfluidics-based SCBC device, we will be able to convert the D2HG amount to fluorescent readouts.

Resazurin immobilization strategies

In our previous studies, we have developed a resazurin analog with an azide pendent (APRz).(Li et al. 2018) We performed surface immobilization of resazurin through a strain-promoted azide-alkyne click reaction, where a single-strand DNA with a dibenzylcyclooctyne moiety served as the linker. Using APRz, NAD^+, diaphorase, and lactate dehydrogenase, we have demonstrated the profiling of lactate production at the single-cell level.(Li et al. 2018) In principle, replacing LDH with D2HGDH should provide a straightforward way of assaying D2HG. However, the synthesis of APRz was challenging,

and the overall yield was low. In addition, APRz contained an azidolysine residue, whose synthesis was dangerous and potentially an explosion hazard. Therefore, we set to develop a new, easier, and safer strategy to achieve resazurin immobilization. A simple method of immobilizing molecular probes onto the surface is to use the streptavidin-biotin complex. Since there are well-established approaches to anchor streptavidin onto the surface through DNA conjugation,(Li et al. 2018; Xue et al. 2015) the challenge here is to develop a suitable resazurin-biotin conjugate.

Because of the strong hydrophobicity of biotin, we reasoned that a hydrophilic linker was necessary to improve the solubility. We first designed a biotin-PEG5-resazurin (BPRz) compound and successfully synthesized it through solid-phase synthetic procedures (Figure 2a, Supplementary Material Figure S1-3). As expected, BPRz was very soluble in water and seemed to be a promising probe. We also found that BPRz had almost the same absorption and fluorescence spectra as those of APRz (Supplementary Material Figure S8),(Li et al. 2018) which was consistent with our prior observations that resazurin analogs shared similar spectroscopic properties.

We then evaluated BPRz's performance in translating D2HG levels to fluorescence readouts via the coupled enzyme reactions. We mixed the BPRz probes with NAD+, diaphorase, D2HGDH, and D2HG standards. The resultant solution was incubated at room temperature, and the fluorescence intensities were continuously measured through the time course. As shown in Figure S9, the fluorescence intensities rose rapidly in the presence of D2HG and reached a plateau after 2 hours, suggesting that the BPRz probe was successfully reduced to its product, BPRf, through the cascade enzyme reactions. In contrast, no noticeable fluorescence signal changes were observed in the absence of D2HG, indicating that no enzyme reaction occurred. These results were consistent with our prior data based on APRz. (Li et al. 2018)

The fluorescence intensities of the generated BPRf products first increased with the increasing D2HG concentrations but dropped to very low levels at high D2HG concentrations. Because BPRf is amphiphilic, we attributed this observed fluorescence loss to a possible self-assembly process, where BPRf molecules interact with each other and caused fluorescence quenching. Nevertheless, since the BPRz probes would be immobilized onto the surface through the biotin-streptavidin interaction, we expected that streptavidin would prevent the self-assembly of BPRf molecules, thereby alleviating the loss of fluorescence at high concentrations. To test our hypothesis, we incubated BPRz with streptavidin to form a stable complex and then used this complex for the cascade enzyme reactions. As shown in Figure 2c, the formation of the BPRz-streptavidin complex gave rise to a continuous increase of fluorescence intensities along with increasing D2HG levels, and no obvious fluorescence quenching existed even at high D2HG concentrations (100 μM). These results supported our hypothesis, suggesting that the BPRf-streptavidin complex formation successfully overcame the self-quenching of BPRf at high concentrations. However, this streptavidin complex's adaption to the D2HG assay resulted in another severe problem – the fluorescence intensities of the reduced product, BPRf-streptavidin, displayed fluorescence intensities that were 100 times lower than those obtained from free BPRz

molecules (Figure 2b, 2c). Consequently, the resulted D2HG assay exhibited an intrinsically low sensitivity, and the BPRz probe was proven not suitable for reliable detection of D2HG.

We reasoned that the observed loss of fluorescence in the presence of streptavidin was mainly derived from the short distance between the streptavidin and the resorufin moieties, which could enable energy transfer and thus quench the fluorescence signal. To verify our hypothesis, we first reduced BPRz to BPRf in solution and then added streptavidin into the mixture. As shown in Figure S9, a significant loss of fluorescence was observed after the formation of the BPRf-streptavidin complex, which was similar to what we observed in the D2HG assay above (Figure 2c). This result indicated that the loss of signal was indeed due to the streptavidin-induced quenching effects.

To mitigate the quenching from streptavidin, we hypothesized that by extending the distance between biotin and resazurin, and thus between streptavidin and resorufin, we could decrease the quenching efficiency and rescue the fluorescence. For this purpose, we designed and synthesized biotin-PEG48-resazurin (BP2Rz, Figure 3a, Supplementary Material Figure S4-6), and compared the fluorescence intensities of the reduced product, BP2Rf, and BP2Rf-streptavidin complex. As shown in Figure S10, the fluorescence intensity largely remained after the formation of the BP2Rf-streptavidin complex, validating our hypothesis that the fluorescence intensity could be recovered by rationally tailoring the distance between streptavidin and resorufin. We then evaluated the performance of the resultant BP2Rz-streptavidin complex in the D2HG assay. As shown in Figure 3b, a monotonic relationship between the fluorescence intensities and D2HG levels was observed. In addition, the fluorescence intensities were hundreds of times higher than those from the BPRz-streptavidin-based D2HG assays, proving that by rationally tailoring the PEG linker, the BP2Rz probes were able to efficiently translate the D2HG levels to sensitive fluorescence readouts with minimal quenching.

We then sought to test if the surface-immobilized BP2Rz-streptavidin complex could be adapted to microfluidic chips for D2HG detection. To this end, we first patterned single-strand DNA oligomers on the surface of a glass slide and subsequently anchored streptavidin-DNA conjugates to the surface. By incubating the BP2Rz solution on the glass slide, we assembled BP2Rz-streptavidin complexes on the surface. We mixed NAD+, diaphorase, D2HGDH, and different concentrations of D2HG and then applied these mixtures onto the glass slide. After two hours, we washed the slides and evaluated the fluorescence. As shown in Figure 3c, the fluorescence intensities correlated well with the D2HG concentration, demonstrating a typical sigmoidal response trend. This response curve was comparable to the one obtained using APRz (Supplementary Material Figure S11), which further validated our design principals. The detection limit of this D2HG assay was calculated to be as low as 2.2 μM. In addition, the expected D2HG levels in single cells were estimated to be around 30 μM in one chamber of the microfluidic chip,(Gross et al. 2010) which can be covered by the dynamic range of the developed D2HG assay.

Since we aimed to quantify D2HG levels directly from lysed cells in the SCBC platform, the potential interferences from other reductive species were also evaluated. As shown in Figure S12, the presence of common intracellular reductive chemicals such as glucose, glutamine,

and ascorbate at their physiological concentrations did not result in obvious changes in the fluorescence signals. The only exception was glutathione, which generated slight signals. Nevertheless, after 2 hours of incubation, the fluorescence from GSH-caused reduction was only 5% of that obtained from the D2HG assay, suggesting that the interference from GSH could be ignored. We then compared the performance of our D2HG assay with a commercially available kit by analyzing the D2HG concentration in BT142 mut/- cell lysate. Our results proved that the accuracy of the BP2Rz-based D2HG assay was comparable to the commercial kit (Supplementary Material Figure S13). Taken together, this surface-based D2HG assay demonstrated good sensitivity, selectivity, accuracy, and compatibility with the microfluidic chip platform, and it was ready to be incorporated into the SCBC platform for multiplexed single-cell analysis.

Single-cell analysis of BT142 mut/- cells

With the BP2Rz-streptavidin system ready, we set to perform single-cell profiling of D2HG, glucose uptake, and a panel of signaling phosphoproteins using BT142 mut/- cells. These cells are human oligoastrocytoma cells carrying an R132H point mutation on the IDH1 enzyme.(Luchman et al. 2012; Mehrjardi et al. 2020) In particular, they grow as neurospheres in culture and resemble the characteristics of glioma tumors harboring IDH1 mutations well. In addition to assaying oncometabolite D2HG and glucose uptake, the analyte panel also included oncogenic phosphoproteins (p-p70S6K, p-EGFR, p-mTOR, p-ERK, p-Src, p-4EBP1, p-AKT) and stress-response proteins (p-NDRG, p53) commonly altered in glioma, as well as a cell proliferation marker (Ki67).(Brennan et al. 2013; Li et al. 2018; Verhaak et al. 2010; Xue et al. 2016; Xue et al. 2015)

The single-cell analysis was performed on the SCBC platform.(Li et al. 2018; Xue et al. 2016; Xue et al. 2015) The SCBC platform consisted of two parts – a two-layer microfluidic device made from polydimethylsiloxane and a glass slide with surface-immobilized DNA barcodes. The microfluidic device could separate single cells in 416 individual chambers, and the access to those chambers was controlled through programmable valves. The device also allowed on-chip cell incubation and cell lysis, both of which were performed without inter-chamber crosstalk (Supplementary Material Figure S7). The glass slide served as the bottom of the chambers, each of which was equipped with a set of DNA barcodes that enabled multiplex fluorescence measurements of the analytes.

As shown in Figure 4, D2HG levels varied significantly among single cells. The distribution of this heterogeneity was similar to those of the signaling proteins but different from glucose uptake. Specifically, we could observe two peaks at $Z = -1$ and $Z = 0$ on the D2HG distribution, indicating two subpopulations. Many of the proteins also exhibited multiple peaks, supporting the hypothesis that there were subpopulations. It is also worth pointing out that, compared with other analytes, p-p70S6K showed considerably less heterogeneity despite a few outliers with extremely high levels ($Z > 10$). Interestingly, this property was resembled by its direct upstream protein, p-mTOR. This lack of heterogeneity hinted that the mTOR-p70S6K signaling axis was well-regulated and constrained in these IDH1 mutant cells and that this axis played critical roles.(Fu et al. 2015)

In order to further study the subpopulations, we performed agglomerative hierarchical clustering (AHC) analysis. We compared the Euclidian distance between the single-cell datapoints and carried out the clustering using Ward's method. This exercise revealed two distinct subpopulations (Figure 5a). Based on the analyte levels in each cluster, we found that many signaling proteins behaved similarly across the dataset. For instance, cells with high p-EGFR levels also had high p-ERK, p-Src, and p-Akt levels. Even though there were a few outliers, p-mTOR, p-NDRG and p-4EBP1 also had similar patterns as those signaling proteins. On the other hand, p-p70S6K exhibited a unique pattern that was different from all analytes. Another interesting finding from the clustering result was that the D2HG levels were not associated with any other analytes, which hinted that the oncogenic signaling was decoupled from D2HG metabolism.

We then evaluated the analyte levels of the cluster centroids (Figure 5b). As expected, most signaling proteins exhibited different levels between the two centroids, and the levels were consistent among them in each centroid. In comparison, the levels of p-p70S6K, p-4EBP1, Ki67, glucose, and D2HG were less separated, indicating that these analytes contributed less to the identification of subpopulations in the AHC process. Nevertheless, it is worth pointing out that the levels of Ki67 did not vary between the two subpopulations. This lack of participation hinted that complex cellular heterogeneity existed within each subpopulation, and a more comprehensive analysis was necessary.

We then performed principal component analysis to better evaluate the contribution of each analyte to the global cellular heterogeneity. As shown in Figure 5c, oncogenic signaling proteins such as p-mTOR, p-EGFR, p-ERK, p-AKT, and p-Src contributed primarily to PC1, while D2HG, glucose, p-70S6K and p-4EBP1 mostly aligned along PC2. This orthogonality between analyte contributions echoed with the AHC results. More importantly, we identified a strong divergence between D2HG and the two mTOR downstream effectors, p-p70S6K and p-4EBP1. This opposing relationship was consistent with prior studies, where elevated D2HG levels led to inhibited mTOR signaling.(Fu et al. 2015) D2HG also diverged from Ki67, which matched D2HG's known role of slowing down cell proliferation.(Fu et al. 2015) Interestingly, both p-p70S6K and p-4EBP1 aligned well with Ki67, hinting at mTOR-signaling's critical role in these cells. However, it is worth pointing out that PC1 and PC2 only covered 70% of the global variance. Indeed, only p-p70S6K stayed well-aligned with Ki67 in PC3 and PC4 (Supplementary Material Figure S14). Taken together, the results from the PCA analysis suggested that p-p70S6K could be a potential target to perturb the cell growth in these cells.

To further delineate the interactions between analytes, we calculated the pairwise Spearman correlations between all 12 analytes. As shown in Figure 5d, the oncogenic signaling network in these cells was highly coordinated, as indicated by the strong correlations between those signaling proteins. We found that D2HG exhibited a strong anticorrelation with p-NDRG, which underscored that high D2HG levels led to increased cellular stress.(Ellen et al. 2008) We also noticed that the glucose uptake levels showed strong anticorrelations with p-EGFR and p-AKT. This result was the opposite of regular glioma cells, highlighting the prominent level of metabolic reprogramming in these *IDH*-mutant cells.(Akhavan et al. 2010; Dang et al. 2009; Li et al. 2018; Xue et al. 2016; Xue et al. 2015)

Nevertheless, the two downstream effectors of mTOR, p-p70S6K and p-4EBP1, still exhibited positive correlations with glucose uptake levels, which was consistent with the results from regular glioma cells.(Akhavan et al. 2010; Xue et al. 2015)

Interestingly, the D2HG level also showed a strong anticorrelation with p-p70S6K, which matched with the results from the PCA analysis (Figure 5c). Because glucose uptake and D2HG levels showed opposite relationships with p-p70S6K, this result hinted that p70S6K was critically involved in, if not directly regulating, the metabolic alterations in these IDH mutant cells. Considering that p-p70S6K also correlated with the cell proliferation marker, Ki67, we hypothesized that targeting p70S6K could inhibit the proliferation of these cells. Moreover, because of the anticorrelation between D2HG and p-p70S6K, blocking the aberrant IDH activities in these cells – a potential therapeutic strategy for treating *IDH*-mutant gliomas currently being tested in clinical trials (Golub et al. 2019; Huang et al. 2019) – may promote compensatory activation of p-p70S6K and cell proliferation. Therefore, we further hypothesized that simultaneous inhibition of p70S6K and IDH activities could achieve synergistic effects for arresting the tumor cell growth.

Ivosidenib and LY2584702 as a synergistic drug combination

To test our hypothesis, we treated the BT142 cells with ivosidenib (an IDH inhibitor, 1 μM), (Roboz et al. 2020) LY2584702 (a p70S6K inhibitor, varying concentrations),(Hollebecque et al. 2014) and a combination of them. After the treatment, we evaluated the corresponding cell viabilities. As shown in Figure 6a, LY2584702 significantly inhibited cell proliferation in a dose-dependent manner, which validated our hypothesis that p70S6K played critical roles in the metabolic reprogramming and cell survival of these *IDH*-mutant cells. In addition, the addition of ivosidenib led to improved efficacies. This result pointed to a potential synergy between IDH inhibition and p70S6K inhibition.

In order to quantitatively evaluate this synergy, we treated the cells with different concentration combinations of those two drugs and then calculated the synergy score based on the BLISS definition of independence. As shown in Figure 6b, there were strong synergistic effects between ivosidenib and LY2584702 across a wide range of concentrations.

4. Conclusion

In conclusion, we established a surface-based detection method for profiling D2HG levels in single cells. The key to this assay was a resazurin analog with an extended PEG linker, which alleviated the quenching effect of streptavidin. The synthesis of this resazurin analog was safe and inexpensive, and the yield was higher than the previously reported analogs. By integrating this D2HG assay into the multiplex SCBC platform, we simultaneously analyzed critical oncogenic signaling proteins, glucose uptake, and D2HG levels in single cells. With this technology, we interrogated interactions between oncogenic protein signaling and accumulated D2HG in BT142 mut/- glioma cells and identified that p70S6K played a critical role in supporting cell proliferation. Based on the single-cell data, we predicted and demonstrated that a combinatory inhibition of p70S6K and mutant IDH could synergistically inhibit cell proliferation. In addition to the D2HG assay presented here, the surface-

immobilized BP2Rz probes may be adapted to quantify other redox-active molecules by implementing different enzymatic reactions.

Supplementary Material

Refer to Web version on PubMed Central for supplementary material.

Acknowledgement

The authors gratefully thank the following funding agencies for financial support: National Institutes of Health R03 CA227352 (W.W and M.X.), U54 CA199090 (W.W. and M.X.), U01 CA217655 (W.W.), and Andy Hill CARE Fund (W.W.).

References

Akhavan D, Cloughesy TF, Mischel PS, 2010. mTOR signaling in glioblastoma: lessons learned from bench to bedside. Neuro Oncol 12(8), 882–889. [PubMed: 20472883]

Almendro V, Marusyk A, Polyak K, 2013. Cellular Heterogeneity and Molecular Evolution in Cancer. Annual Review of Pathology: Mechanisms of Disease 8(1), 277–302.

Altman BJ, Stine ZE, Dang CV, 2016. From Krebs to clinic: glutamine metabolism to cancer therapy. Nature Reviews Cancer 16(10), 619–634. [PubMed: 27492215]

Balss J, Pusch S, Beck A-C, Herold-Mende C, Krämer A, Thiede C, Buckel W, Langhans C-D, Okun JG, von Deimling A, 2012. Enzymatic assay for quantitative analysis of (d)-2-hydroxyglutarate. Acta Neuropathologica 124(6), 883–891. [PubMed: 23117877]

Brennan Cameron W., Verhaak Roel G.W., McKenna A, Campos B, Noushmehr H, Salama Sofie R., Zheng S, Chakravarty D, Sanborn JZ, Berman Samuel H., Beroukhim R, Bernard B, Wu C-J, Genovese G, Shmulevich I, Barnholtz-Sloan J, Zou L, Vegesna R, Shukla Sachet A., Ciriello G, Yung WK, Zhang W, Sougnez C, Mikkelsen T, Aldape K, Bigner Darell D., Van Meir Erwin G., Prados M, Sloan A, Black Keith L., Eschbacher J, Finocchiaro G, Friedman W, Andrews David W., Guha A, Iacocca M, O'Neill Brian P., Foltz G, Myers J, Weisenberger Daniel J., Penny R, Kucherlapati R, Perou Charles M., Hayes DN, Gibbs R, Marra M, Mills Gordon B., Lander E, Spellman P, Wilson R, Sander C, Weinstein J, Meyerson M, Gabriel S, Laird Peter W., Haussler D, Getz G, Chin L, Benz C, Barnholtz-Sloan J, Barrett W, Ostrom Q, Wolinsky Y, Black Keith L., Bose B, Boulos Paul T., Boulos M, Brown J, Czerinski C, Eppley M, Iacocca M, Kempista T, Kitko T, Koyfman Y, Rabeno B, Rastogi P, Sugarman M, Swanson P, Yalamanchii K, Otey Ilana P., Liu Yingchun S., Xiao Y, Auman JT, Chen P-C, Hadjipanayis A, Lee E, Lee S, Park Peter J., Seidman J, Yang L, Kucherlapati R, Kalkanis S, Mikkelsen T, Poisson Laila M., Raghunathan A, Scarpace L, Bernard B, Bressler R, Eakin A, Iype L, Kreisberg Richard B., Leinonen K, Reynolds S, Rovira H, Thorsson V, Shmulevich I, Annala Matti J., Penny R, Paulauskis J, Curley E, Hatfield M, Mallery D, Morris S, Shelton T, Shelton C, Sherman M, Yena P, Cuppini L, DiMeco F, Eoli M, Finocchiaro G, Maderna E, Pollo B, Saini M, Balu S, Hoadley Katherine A., Li L, Miller CR, Shi Y, Topal Michael D., Wu J, Dunn G, Giannini C, O'Neill Brian P., Aksoy BA, Antipin Y, Borsu L, Berman Samuel H., Brennan Cameron W., Cerami E, Chakravarty D, Ciriello G, Gao J, Gross B, Jacobsen A, Ladanyi M, Lash A, Liang Y, Reva B, Sander C, Schultz N, Shen R, Socci Nicholas D., Viale A, Ferguson Martin L., Chen Q-R, Demchok John A., Dillon Laura A.L., Shaw Kenna R.M., Sheth M, Tarnuzzer R, Wang Z, Yang L, Davidsen T, Guyer Mark S., Ozenberger Bradley A., Sofia Heidi J., Bergsten J, Eckman J, Harr J, Myers J, Smith C, Tucker K, Winemiller C, Zach Leigh A., Ljubimova Julia Y., Eley G, Ayala B, Jensen Mark A., Kahn A, Pihl Todd D., Pot David A., Wan Y, Eschbacher J, Foltz G, Hansen N, Hothi P, Lin B, Shah N, Yoon J.-g., Lau C, Berens M, Ardlie K, Beroukhim R, Carter Scott L., Cherniack Andrew D., Noble M, Cho J, Cibulskis K, DiCara D, Frazer S, Gabriel Stacey B., Gehlenborg N, Gentry J, Heiman D, Kim J, Jing R, Lander Eric S., Lawrence M, Lin P, Mallard W, Meyerson M, Onofrio Robert C., Saksena G, Schumacher S, Sougnez C, Stojanov P, Tabak B, Voet D, Zhang H, Zou L, Getz G, Dees Nathan N., Ding L, Fulton Lucinda L., Fulton Robert S., Kanchi K-L, Mardis Elaine R., Wilson Richard K., Baylin Stephen B., Andrews David W., Harshyne L, Cohen Mark L., Devine K, Sloan Andrew E., VandenBerg Scott

R., Berger Mitchel S., Prados M, Carlin D, Craft B, Ellrott K, Goldman M, Goldstein T, Grifford M, Haussler D, Ma S, Ng S, Salama Sofie R., Sanborn JZ, Stuart J, Swatloski T, Waltman P, Zhu J, Foss R, Frentzen B, Friedman W, McTiernan R, Yachnis A, Hayes DN, Perou Charles M., Zheng S, Vegesna R, Mao Y, Akbani R, Aldape K, Bogler O, Fuller Gregory N., Liu W, Liu Y, Lu Y, Mills G, Protopopov A, Ren X, Sun Y, Wu C-J, Yung WKA, Zhang W, Zhang J, Chen K, Weinstein John N., Chin L, Verhaak Roel G.W., Noushmehr H, Weisenberger Daniel J., Bootwalla Moiz S., Lai Phillip H., Triche Timothy J. Jr., Van Den Berg David J., Laird Peter W., Gutmann David H., Lehman Norman L., VanMeir Erwin G., Brat D, Olson Jeffrey J., Mastrogianakis Gena M., Devi Narra S., Zhang Z, Bigner D, Lipp E, McLendon R, 2013. The Somatic Genomic Landscape of Glioblastoma. Cell 155(2), 462–477. [PubMed: 24120142]

Cairns RA, Harris IS, Mak TW, 2011. Regulation of cancer cell metabolism. Nature Reviews Cancer 11(2), 85–95. [PubMed: 21258394]

Dang L, White DW, Gross S, Bennett BD, Bittinger MA, Driggers EM, Fantin VR, Jang HG, Jin S, Keenan MC, Marks KM, Prins RM, Ward PS, Yen KE, Liau LM, Rabinowitz JD, Cantley LC, Thompson CB, Vander Heiden MG, Su SM, 2009. Cancer-associated IDH1 mutations produce 2-hydroxyglutarate. Nature 462(7274), 739–744. [PubMed: 19935646]

DeBerardinis Ralph J., Thompson Craig B., 2012. Cellular Metabolism and Disease: What Do Metabolic Outliers Teach Us? Cell 148(6), 1132–1144. [PubMed: 22424225]

Ellen TP, Ke Q, Zhang P, Costa M, 2008. NDRG1, a growth and cancer related gene: regulation of gene expression and function in normal and disease states. Carcinogenesis 29(1), 2–8. [PubMed: 17916902]

Fan J, Teng X, Liu L, Mattaini KR, Looper RE, Vander Heiden MG, Rabinowitz JD, 2015. Human phosphoglycerate dehydrogenase produces the oncometabolite D-2-hydroxyglutarate. ACS Chem Biol 10(2), 510–516. [PubMed: 25406093]

Fu X, Chin Randall M., Vergnes L, Hwang H, Deng G, Xing Y, Pai Melody Y., S., Ta L, Fazlollahi F, Chen C, Prins Robert M., Teitell Michael A., Nathanson David A., Lai A, Faull Kym F., Jiang M, Clarke Steven G., Cloughesy Timothy F., Graeber Thomas G., Braas D, Christofk Heather R., Jung Michael E., Reue K, Huang J, 2015. 2-Hydroxyglutarate Inhibits ATP Synthase and mTOR Signaling. Cell Metabolism 22(3), 508–515. [PubMed: 26190651]

Golub D, Iyengar N, Dogra S, Wong T, Bready D, Tang K, Modrek AS, Placantonakis DG, 2019. Mutant Isocitrate Dehydrogenase Inhibitors as Targeted Cancer Therapeutics. Frontiers in Oncology 9, 417. [PubMed: 31165048]

Gross S, Cairns RA, Minden MD, Driggers EM, Bittinger MA, Jang HG, Sasaki M, Jin S, Schenkein DP, Su SM, Dang L, Fantin VR, Mak TW, 2010. Cancer-associated metabolite 2-hydroxyglutarate accumulates in acute myelogenous leukemia with isocitrate dehydrogenase 1 and 2 mutations. Journal of Experimental Medicine 207(2), 339–344.

Heath JR, Ribas A, Mischel PS, 2016. Single-cell analysis tools for drug discovery and development. Nature Reviews Drug Discovery 15(3), 204–216. [PubMed: 26669673]

Hollebecque A, Houédé N, Cohen EEW, Massard C, Italiano A, Westwood P, Bumgardner W, Miller J, Brail LH, Benhadji KA, Soria J-C, 2014. A phase Ib trial of LY2584702 tosylate, a p70 S6 inhibitor, in combination with erlotinib or everolimus in patients with solid tumours. European Journal of Cancer 50(5), 876–884. [PubMed: 24456794]

Huang J, Yu J, Tu L, Huang N, Li H, Luo Y, 2019. Isocitrate Dehydrogenase Mutations in Glioma: From Basic Discovery to Therapeutics Development. Frontiers in Oncology 9, 506. [PubMed: 31263678]

Krzywinski M, Schein J, Birol I, Connors J, Gascoyne R, Horsman D, Jones SJ, Marra MA, 2009. Circos: an information aesthetic for comparative genomics. Genome Res 19(9), 1639–1645. [PubMed: 19541911]

Kwong GA, Radu CG, Hwang K, Shu CJ, Ma C, Koya RC, Comin-Anduix B, Hadrup SR, Bailey RC, Witte ON, Schumacher TN, Ribas A, Heath JR, 2009. Modular Nucleic Acid Assembled p/MHC Microarrays for Multiplexed Sorting of Antigen-Specific T Cells. Journal of the American Chemical Society 131(28), 9695–9703. [PubMed: 19552409]

Li Z, Cheng H, Shao S, Lu X, Mo L, Tsang J, Zeng P, Guo Z, Wang S, Nathanson DA, Heath JR, Wei W, Xue M, 2018. Surface Immobilization of Redox-Labile Fluorescent Probes: Enabling Single-

Cell Co-Profiling of Aerobic Glycolysis and Oncogenic Protein Signaling Activities. Angewandte Chemie International Edition 57(36), 11554–11558. [PubMed: 29992724]

Li Z, Wang Z, Tang Y, Lu X, Chen J, Dong Y, Wu B, Wang C, Yang L, Guo Z, Xue M, Lu S, Wei W, Shi Q, 2019. Liquid biopsy-based single-cell metabolic phenotyping of lung cancer patients for informative diagnostics. Nature Communications 10(1), 3856.

Lin A-P, Abbas S, Kim S-W, Ortega M, Bouamar H, Escobedo Y, Varadarajan P, Qin Y, Sudderth J, Schulz E, Deutsch A, Mohan S, Ulz P, Neumeister P, Rakheja D, Gao X, Hinck A, Weintraub ST, DeBerardinis RJ, Sill H, Dahia PLM, Aguiar RCT, 2015. D2HGDH regulates alpha-ketoglutarate levels and dioxygenase function by modulating IDH2. Nature Communications 6(1), 7768.

Loenarz C, Schofield CJ, 2008. Expanding chemical biology of 2-oxoglutarate oxygenases. Nature Chemical Biology 4(3), 152–156. [PubMed: 18277970]

Luchman HA, Stechishin OD, Dang NH, Blough MD, Chesnelong C, Kelly JJ, Nguyen SA, Chan JA, Weljie AM, Cairncross JG, Weiss S, 2012. An in vivo patient-derived model of endogenous IDH1-mutant glioma. Neuro Oncol 14(2), 184–191. [PubMed: 22166263]

Mehrjardi NZ, Hänggi D, Kahlert UD, 2020. Current biomarker-associated procedures of cancer modeling-a reference in the context of IDH1 mutant glioma. Cell Death & Disease 11(11), 998. [PubMed: 33221817]

Mondesir J, Willekens C, Touat M, de Botton S, 2016. IDH1 and IDH2 mutations as novel therapeutic targets: current perspectives. J Blood Med 7, 171–180. [PubMed: 27621679]

Mullen AR, DeBerardinis RJ, 2012. Genetically-defined metabolic reprogramming in cancer. Trends in Endocrinology & Metabolism 23(11), 552–559. [PubMed: 22858391]

Nowell PC, 1976. The clonal evolution of tumor cell populations. Science 194(4260), 23. [PubMed: 959840]

Pavlova Natalya N., Thompson Craig B., 2016. The Emerging Hallmarks of Cancer Metabolism. Cell Metabolism 23(1), 27–47. [PubMed: 26771115]

Polyak K, 2014. Tumor Heterogeneity Confounds and Illuminates: A case for Darwinian tumor evolution. Nature Medicine 20(4), 344–346.

Quail DF, Joyce JA, 2013. Microenvironmental regulation of tumor progression and metastasis. Nature medicine 19(11), 1423–1437.

Reznik GO, Vajda S, Cantor CR, Sano T, 2001. A Streptavidin Mutant Useful for Directed Immobilization on Solid Surfaces. Bioconjugate Chemistry 12(6), 1000–1004. [PubMed: 11716692]

Roboz GJ, DiNardo CD, Stein EM, de Botton S, Mims AS, Prince GT, Altman JK, Arellano ML, Donnellan W, Erba HP, Mannis GN, Pollyea DA, Stein AS, Uy GL, Watts JM, Fathi AT, Kantarjian HM, Tallman MS, Choe S, Dai D, Fan B, Wang H, Zhang V, Yen KE, Kapsalis SM, Hickman D, Liu H, Agresta SV, Wu B, Attar EC, Stone RM, 2020. Ivosidenib induces deep durable remissions in patients with newly diagnosed IDH1-mutant acute myeloid leukemia. Blood 135(7), 463–471. [PubMed: 31841594]

Schulze A, Harris AL, 2012. How cancer metabolism is tuned for proliferation and vulnerable to disruption. Nature 491(7424), 364–373. [PubMed: 23151579]

Tahiliani M, Koh KP, Shen Y, Pastor WA, Bandukwala H, Brudno Y, Agarwal S, Iyer LM, Liu DR, Aravind L, Rao A, 2009. Conversion of 5-methylcytosine to 5-hydroxymethylcytosine in mammalian DNA by MLL partner TET1. Science (New York, N.Y.) 324(5929), 930–935.

Thompson CB, 2009. Metabolic enzymes as oncogenes or tumor suppressors. N Engl J Med 360(8), 813–815. [PubMed: 19228626]

Tsukada Y. i., Fang J, Erdjument-Bromage H, Warren ME, Borchers CH, Tempst P, Zhang Y, 2006. Histone demethylation by a family of JmjC domain-containing proteins. Nature 439(7078), 811–816. [PubMed: 16362057]

Vander Heiden MG, Cantley LC, Thompson CB, 2009. Understanding the Warburg Effect: The Metabolic Requirements of Cell Proliferation. Science 324(5930), 1029. [PubMed: 19460998]

Verhaak RGW, Hoadley KA, Purdom E, Wang V, Qi Y, Wilkerson MD, Miller CR, Ding L, Golub T, Mesirov JP, Alexe G, Lawrence M, O'Kelly M, Tamayo P, Weir BA, Gabriel S, Winckler W, Gupta S, Jakkula L, Feiler HS, Hodgson JG, James CD, Sarkaria JN, Brennan C, Kahn A, Spellman PT, Wilson RK, Speed TP, Gray JW, Meyerson M, Getz G, Perou CM, Hayes DN, 2010. Integrated

Genomic Analysis Identifies Clinically Relevant Subtypes of Glioblastoma Characterized by Abnormalities in PDGFRA, IDH1, EGFR, and NF1. Cancer Cell 17(1), 98–110. [PubMed: 20129251]

Ward Patrick S., Thompson Craig B., 2012. Metabolic Reprogramming: A Cancer Hallmark Even Warburg Did Not Anticipate. Cancer Cell 21(3), 297–308. [PubMed: 22439925]

Xu W, Yang H, Liu Y, Yang Y, Wang P, Kim S-H, Ito S, Yang C, Wang P, Xiao M-T, Liu L. x., Jiang W. q., Liu J, Zhang J. y., Wang B, Frye S, Zhang Y, Xu Y. h., Lei Q. y., Guan K-L, Zhao S. m., Xiong Y, 2011. Oncometabolite 2-Hydroxyglutarate Is a Competitive Inhibitor of α-Ketoglutarate-Dependent Dioxygenases. Cancer Cell 19(1), 17–30. [PubMed: 21251613]

Xue M, Wei W, Su Y, Johnson D, Heath JR, 2016. Supramolecular Probes for Assessing Glutamine Uptake Enable Semi-Quantitative Metabolic Models in Single Cells. J Am Chem Soc 138(9), 3085–3093. [PubMed: 26916347]

Xue M, Wei W, Su Y, Kim J, Shin YS, Mai WX, Nathanson DA, Heath JR, 2015. Chemical methods for the simultaneous quantitation of metabolites and proteins from single cells. J Am Chem Soc 137(12), 4066–4069. [PubMed: 25789560]

Yang M, Soga T, Pollard PJ, 2013. Oncometabolites: linking altered metabolism with cancer. J Clin Invest 123(9), 3652–3658. [PubMed: 23999438]

Ye D, Ma S, Xiong Y, Guan K-L, 2013. R-2-Hydroxyglutarate as the Key Effector of IDH Mutations Promoting Oncogenesis. Cancer Cell 23(3), 274–276. [PubMed: 23518346]

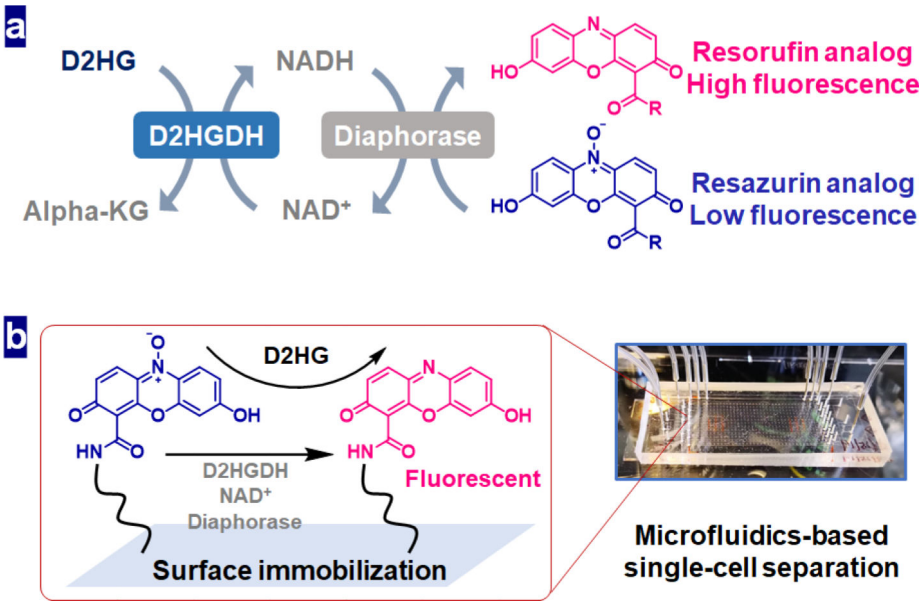

Figure 1.

The detection scheme of the D2HG assay. **a)** Coupled enzymatic reactions convert D2HG to αKG, while generating highly fluorescent resorufin compounds. **b)** Surface immobilization of the resazurin analog and miniaturizing the coupled enzymatic reactions onto the microfluidics-based SCBC device enables the detection of D2HG at the single-cell level.

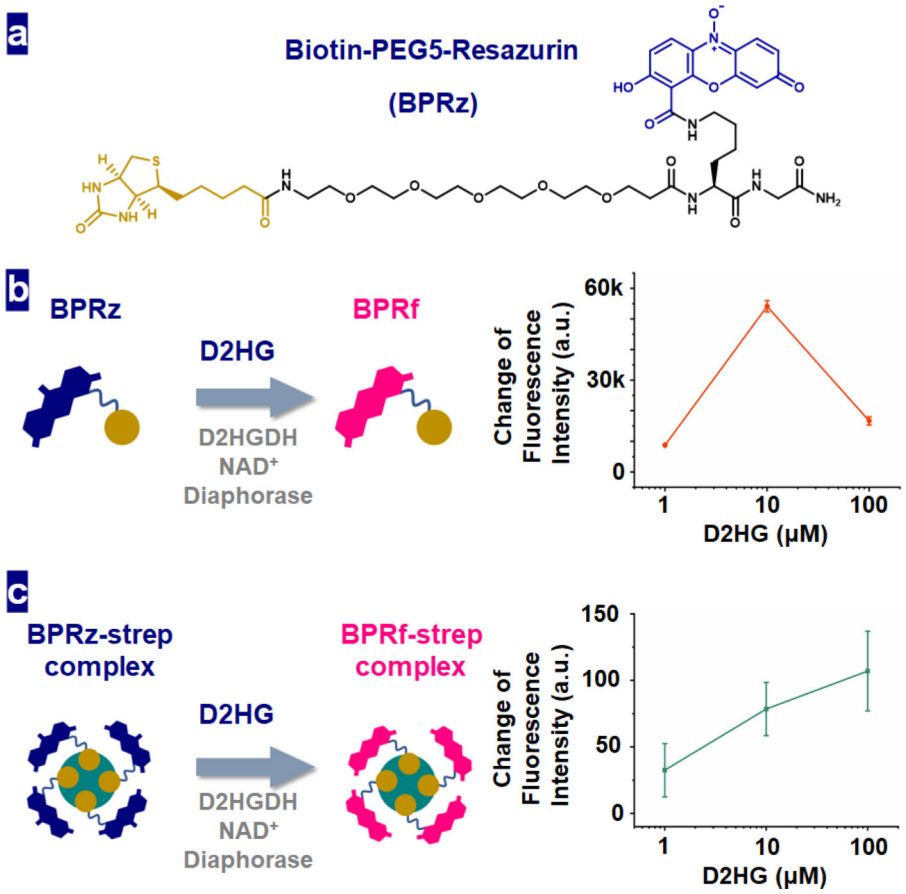

Figure 2.

a) The structure of BPRz. **b)** Left – coupled enzymatic reactions convert non-fluorescent BPRz to fluorescent BPRf; right – BPRz response curve generated by using different concentrations of D2HG. **c)** Left – BPRz conjugated with streptavidin can be converted to BPRf through the same enzymatic reactions; right – BPRz-Strep conjugate response curve generated by using different concentrations of D2HG.

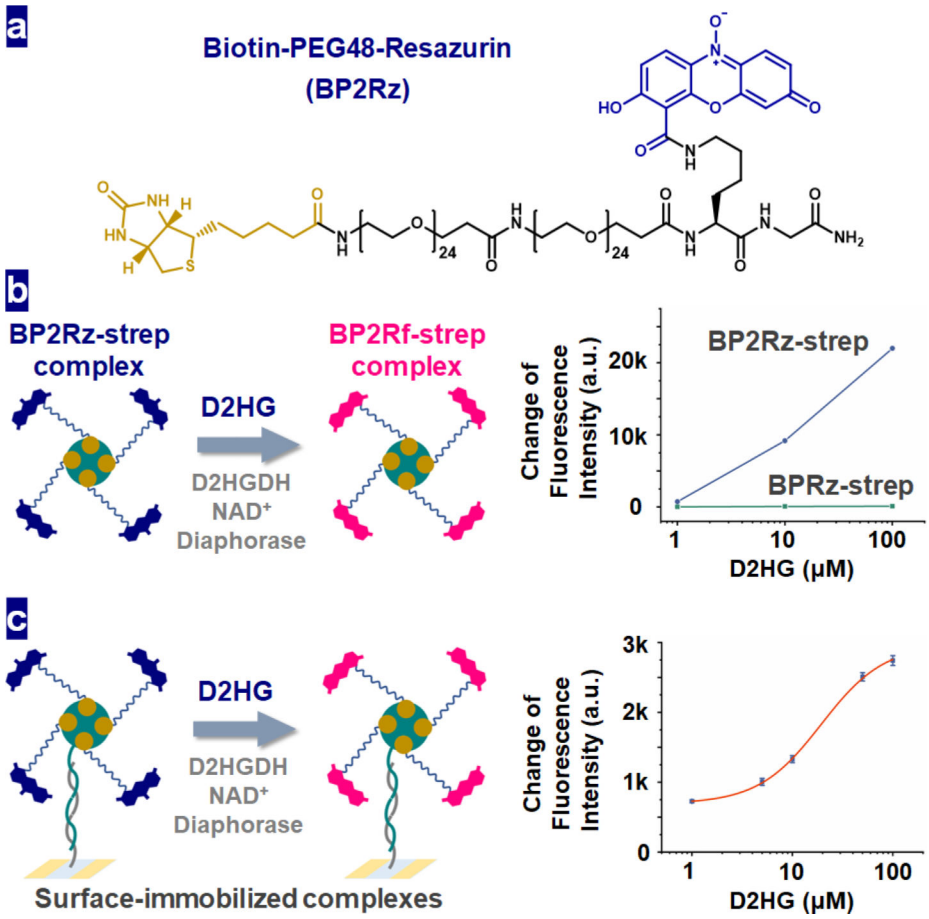

Figure 3.

a) The structure of BP2Rz. **b)** Left – coupled enzymatic reactions convert non-fluorescent BP2Rz-streptavidin complex to fluorescent BP2Rf-streptavidin complex; right – BP2Rz-streptavidin complex response curve generated by using different concentrations of D2HG. The results from using BPRz-streptavidin were included for comparison. The error bars were too small to be visible in the graph. **c)** Left – the BP2Rz-streptavidin complex could be immobilized onto the surface through a DNA linker; right – surface-immobilized BP2Rz-strep complex response curve generated by using different concentrations of D2HG. The red curve was generated by fitting the data points using a Hill function.

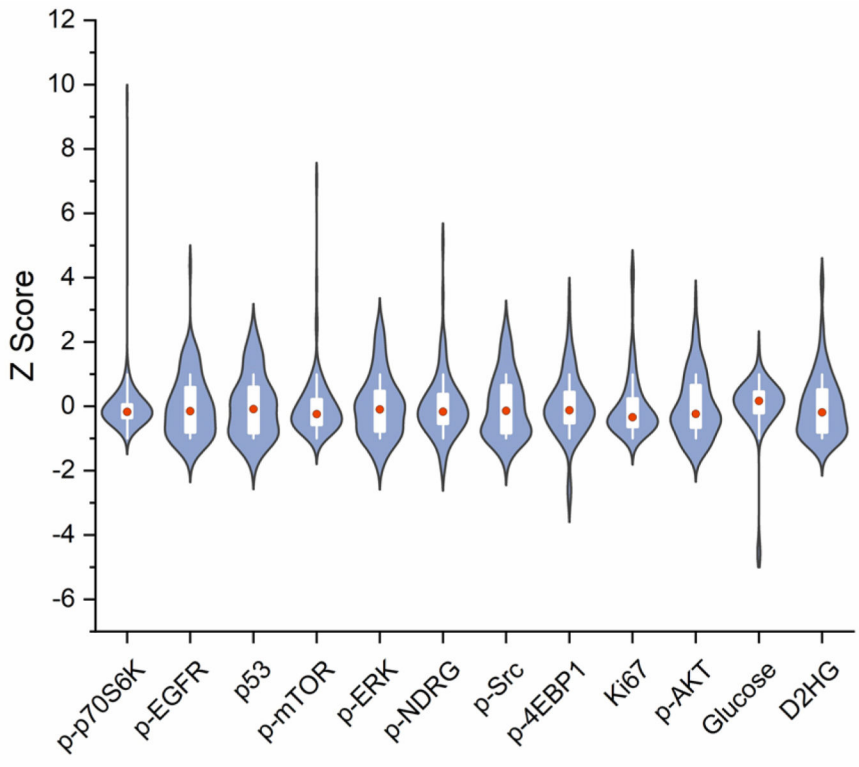

Figure 4.

Multiplex single-cell dataset obtained from BT142 mut/- cells. The violin plots depict the standardized analyte level distributions. The boxes represent the 25%−75% data ranges, and the whiskers show the standard deviations. The red dots label the median values. A total of 108 single cells were included in the experiment.

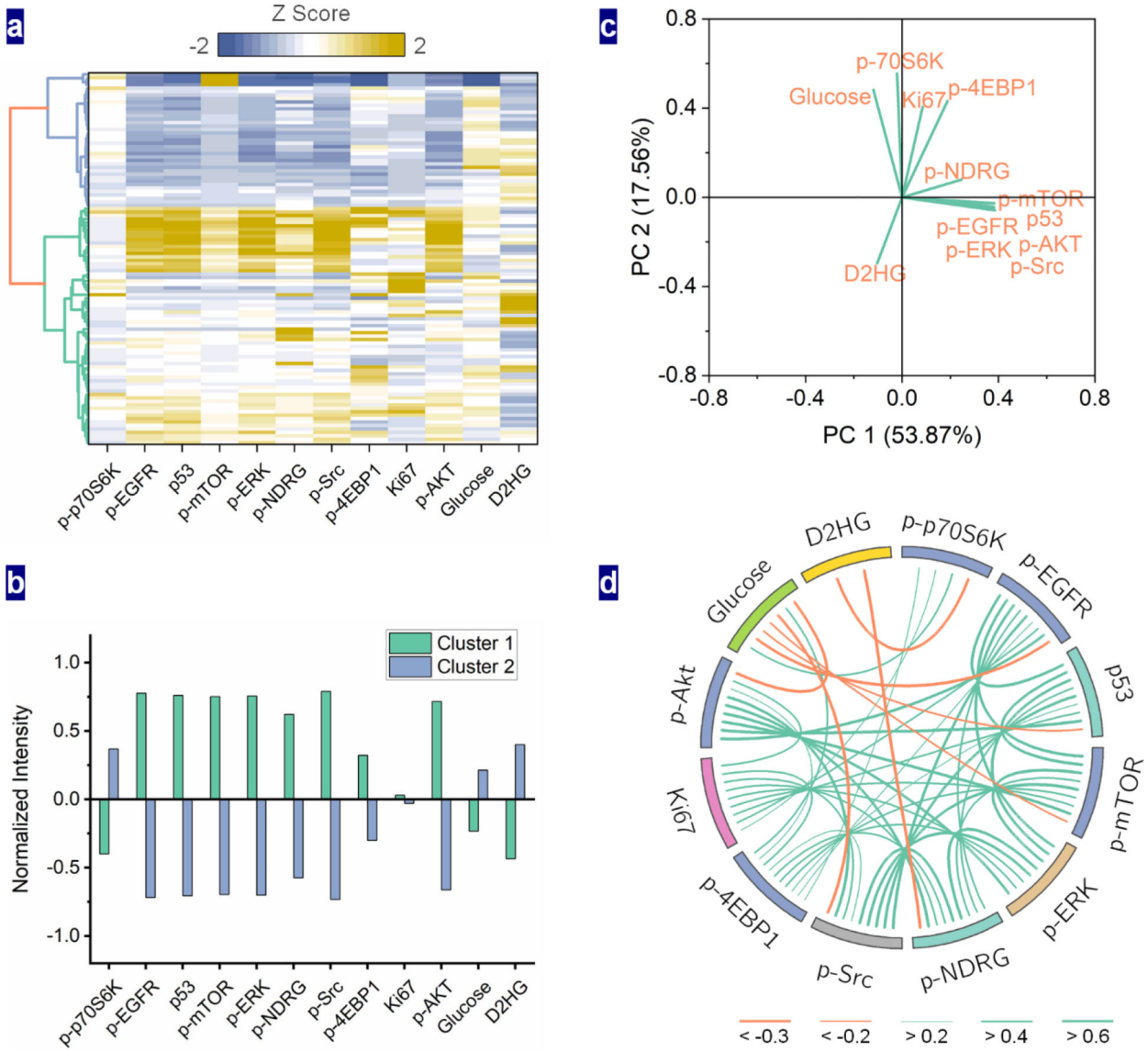

Figure 5.

a) Agglomerative hierarchical clustering result of the single-cell dataset. The heatmap shows the analyte levels as well as the cluster identity of each data point. Two subpopulations were identified. **b)** Analyte levels of the cluster centroids. **c)** Loading plot of PC1 and PC2 from principal component analysis of the single-cell dataset. **d)** The correlation network of the analytes. Green and orange lines represent positive and negative correlations, respectively. The thickness of the lines corresponds with the correlation levels.

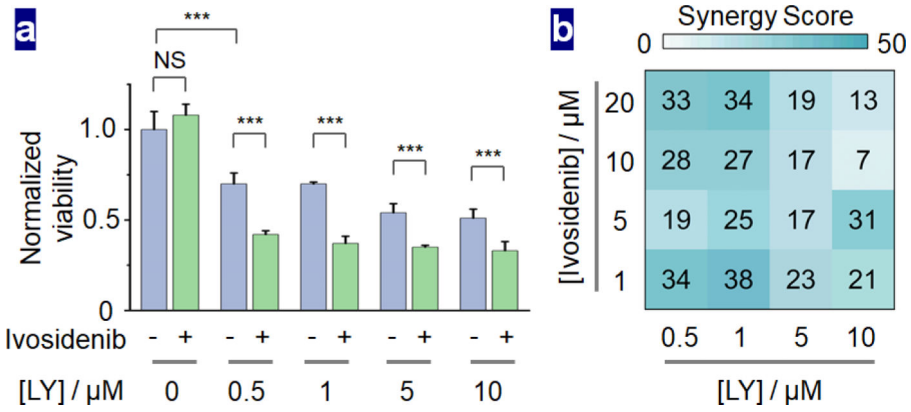

Figure 6.

a) BT142 mut/- cell viabilities as the result of LY2584702 (LY, p70S6K inhibitor) and ivosidenib (IDH1 inhibitor, 1 μM) treatments. NS, not significant. ***, $p < 0.001$. **b)** Synergy scores calculated from the BLISS method across different concentrations of LY and ivosidenib combinations.